Geophysical Research Letters

Supporting Information for

Platelet Ice under Arctic Pack Ice in Winter

Christian Katlein[1*], Volker Mohrholz[2], Igor Sheikin[3], Polona Itkin[4], Dmitry V. Divine[5], Julienne Stroeve[6,7], Arttu Jutila[1], Daniela Krampe[1], Egor Shimanchuk[3], Ian Raphael[8], Benjamin Rabe[1], Ivan Kuznetsov[1], Maria Mallet[1], Hailong Liu[9], Mario Hoppmann[1], Ying-Chih Fang[1], Adela Dumitrascu[10], Stefanie Arndt[1], Philipp Anhaus[1], Marcel Nicolaus[1], Ilkka Matero[1], Marc Oggier[11], Hajo Eicken[11], Christian Haas[1]

[1]Alfred-Wegener-Institute Helmholtz Center for Polar and Marine Research, Bremerhaven, Germany

[2]Institut für Ostseeforschung, Warnemünde, Germany.

[3]Arctic and Antarctic Research Institute, St.Petersburg, Russia

[4]UiT University of Tromsø, Tromsø, Norway

[5]Norwegian Polar Institute, Tromsø, Norway

[6]University College of London, London, United Kingdom

[7]Center for Earth Observation Science, Department of Environment & Geography, University of Manitoba, Winnipeg, MB, Canada

[8]Thayer School of Engineering, Dartmouth College, Hanover NH, United States of America

[9]Shanghai Jiao Tong University, Shanghai, China

[10]University of Gothenburg, Gothenburg, Sweden

[11]International Arctic Research Center, University of Alaska Fairbanks, Fairbanks AK, United States of America

Contents of this file

Introduction

This supplementary information provides additional text and graphics – mostly images – to further illustrate the platelet ice observations described in the main paper. All raw data used in this study are archived in the MOSAiC Central Storage (MCS) according to the MOSAiC Data Policy at the Alfred-Wegener-Institute (AWI) and will be accessible unrestricted after the 1 January 2023.

Text S1: Precision of CTD instruments

The observed supercooling of 10 to 20 mK is close to the uncertainty of the used instruments. Typical uncertainties for temperature, pressure, and salinity derived from conductivity sensors are 5 mK, 0.2 dbar and 0.01 g/kg, respectively. All instruments were calibrated prior to the expedition in calibration labs of the particular manufacturer. The pressure sensor of the MSS was checked by comparing data collected in air above the surface. The observed offset was applied during post processing. The temperature sensors of the MSS were checked against a Seabird SBE911+ CTD system. For this purpose the MSS was mounted on the CTD/rosette frame to gather a concurrent profile of both instruments in the upper 200 m. The SBE911+ will only be finally calibrated several months after the MOSAiC expedition using an analysis of water samples from the rosette with a high-precision salinometer, and calibration of the temperature and conductivity sensors by the manufacturer. Hence, we will only be able to carry out our cross-calibration after that time.
The MSS consists of two temperature sensors, a high precise PT100 and a fast FP07. The sensors were calibrated by Sea & Sun Technology GmbH on 25 May 2019. The calibration range of both temperature sensors is 0 to 30°C. Although, the surface temperature was about -1.7°C and beyond the calibration range, the very linear characteristic of the platinum wire PT100 sensor allow reliable measurements in this range. The uncertainties of the PT100 and the FP07 after the calibration were given by the manufacturer with 2 mK. The uncertainties of pressure and conductivity sensor were given with 0.05 dbar and 0.001 mS/cm, respectively.

The in-situ freezing temperature was calculated with TEOS-10 toolbox GWS [*McDougall and Barker*, 2011]. It depends on absolute salinity and pressure. A salinity uncertainty of 0.01 g/kg results in an uncertainty of freezing temperature of 0.5 mK. The pressure uncertainty of 0.2 dbar causes a freezing temperature uncertainty of 0.15 mK. Thus, the uncertainty of the calculated freezing temperature is not critical, and lower than 1mK.
By using two independent temperature sensors, with different physical measuring principles (platinum wire, and NTC semiconductor element) a failure or drift of one sensor is easily observed. It is very unlikely that both sensors depict the same bias or drift concurrently. To check the sensors the FP07 readings were low pass filtered with the time constant of the PT100. Then the difference between both sensors was calculated. During our campaign no significant change of the temperature difference between both sensors was observed. Thus, we assume an uncertainty of the MSS temperature readings below 5 mK.

Icing of the sensors in supercooled water was not observed, and is highly unlikely. The MSS was operated from a heated tent with about 5°C. Each MSS deployment consists of four to ten subsequent profiles down to 400 m depth. Since only the upper 15 to 25 m are below the in-

situ freezing temperature the probe is most of the time (>93%) in warmer water layers. The time in the supercooled surface layer was 80 to 90 s for each profile.

Several salinity and temperature measurements used in this study are from autonomous ice-tethered instrument systems (hereafter named “buoys”). These buoys contain a surface unit for data telemetry (IRIDIUM) and position (GPS), a 100 m long conducting tether, a terminal weight and five inductive Seabird Microcat CTD (SBE 37IM) between the end of the tether and 10 m water depth. The full buoys (model PacificGyre SVP5S) were custom-designed in cooperation with the Alfred-Wegener-Institute and manufactured by Pacific Gyre Inc. (Oceanside, USA). The Microcat CTD were calibrated by Seabird prior to assembly into the buoy. For the SBE 37IM the manufacturer states an accuracy for the temperature sensor of ± 2mK and a resolution of 0. 1 mK with a stability of 0. 2 mK per month. This results in a maximum expected error of about 5 mK, similar to that of the MSS. The salinity and pressure errors result in an error in the freezing temperature that is similarly negligible as for the MSS. The uppermost CTD in all buoys reported such a low temperature, giving further confidence in our observations of supercooling.
Several profiles with a small, mobile CTD system were obtained nearby some of those buoys throughout the year. This will be used for cross-calibration several months after the MOSAiC expedition, once all main CTD systems used during MOSAiC have been finally calibrated. Even without final calibration, we can say with similar confidence as for the MSS data that we measured supercooled water, as presented in this work.

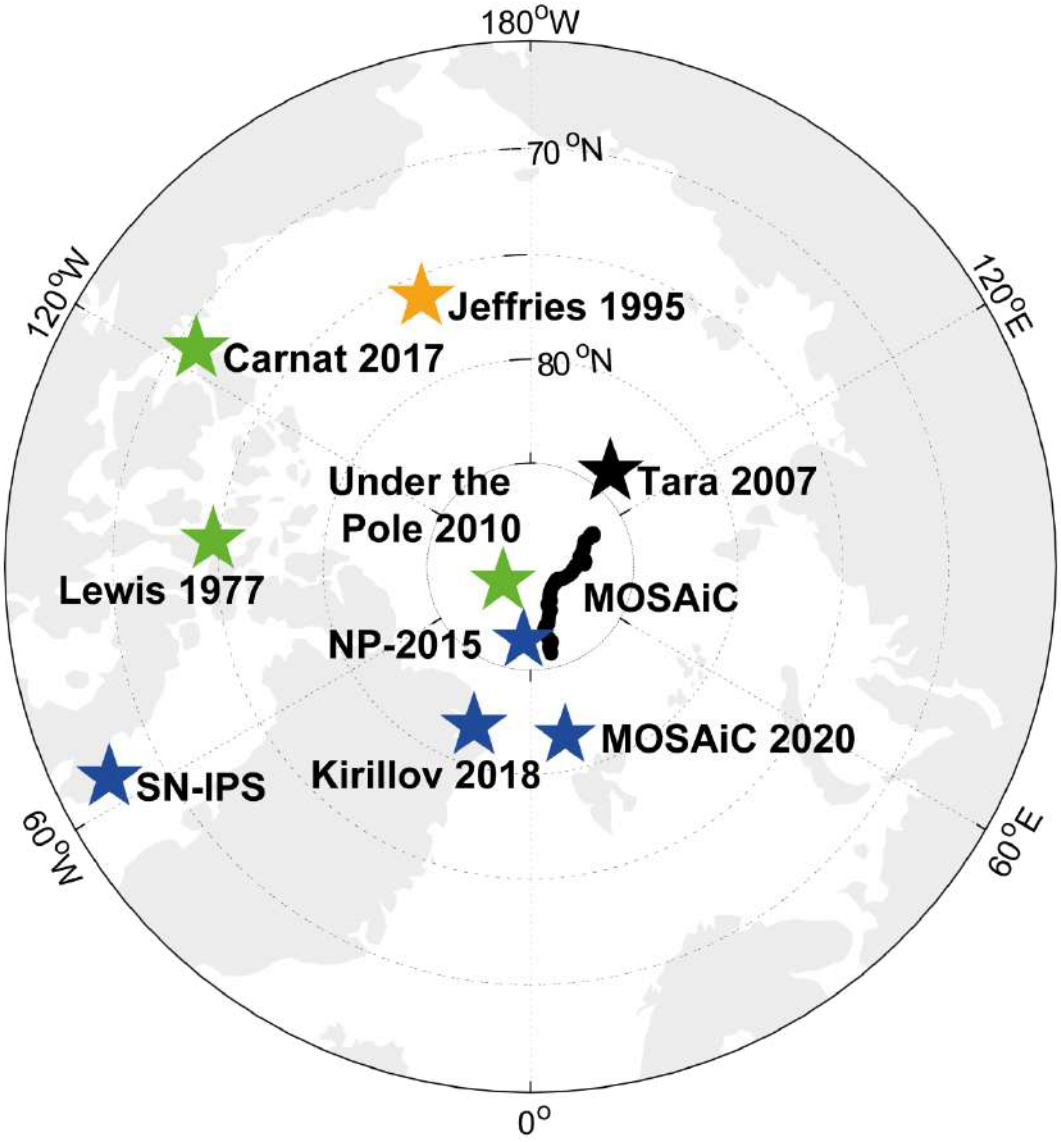

Figure S1. Map showing previous observations of platelet ice with their geographic reference and season (stars indicate location and black, green, blue, orange colors the winter, spring, summer, fall season, respectively). Seasons are indicated as platelet ice formation in summer will in most cases result from meltwater percolation, and thus an entirely different process. The black line shows the track during which platelet ice was observed in this study. Observation references and details can be found in Table ST1.

Table ST1. Collection of previous descriptions of platelet ice in the Arctic. The table includes all observations known to the authors, excluding observations that are explicitly described as false bottom formations in under-ice melt-ponds. It should be noted that most summer season observations likely differ significantly in formation mechanism from our winter observations presented in this study. This also applies to the observation of melt-induced sub-ice platelet layer formation observed on the MOSAiC floe in the end of June 2020.

Work	Reference	Region	Season	Comment
Lewis et al.	*[Lewis and Milne, 1977]*	Resolute Bay (?)	April (?)	time and region not explicitly specified
Jeffries et al.	*[Jeffries et al., 1995]*	Beaufort Sea	August/ September	second and multi-year ice cores
Tara drift	*[Ragobert et al., 2008]*	Central Arctic	Winter	diving observations
"Under the Pole" expedition	*[Bardout et al., 2011]*	Central Arctic	April	exact location unclear
North Pole-2015	*I. Sheikin personal observation*	Central Arctic	July	underwater camera observation
Carnat et al.	*[Carnat et al., 2017]*	Amundsen Gulf	mid-March & mid-May	ice cores - before melt-onset
Kirilov et al.	*[Kirillov et al., 2018]*	Wandel Sea	July/August	indirect buoy observation
Sentinel North – IPS 2018 (CCGS Amundsen)	*C. Katlein personal observation*	southern Baffin Bay	July	edges of melted-through melt ponds
MOSAiC Leg 4	*G. Castellani personal communication*	Northern Fram Strait	end-June	formed after significant surface melt.
MOSAiC Leg 2&3	*this study*	Central Arctic	December to March	

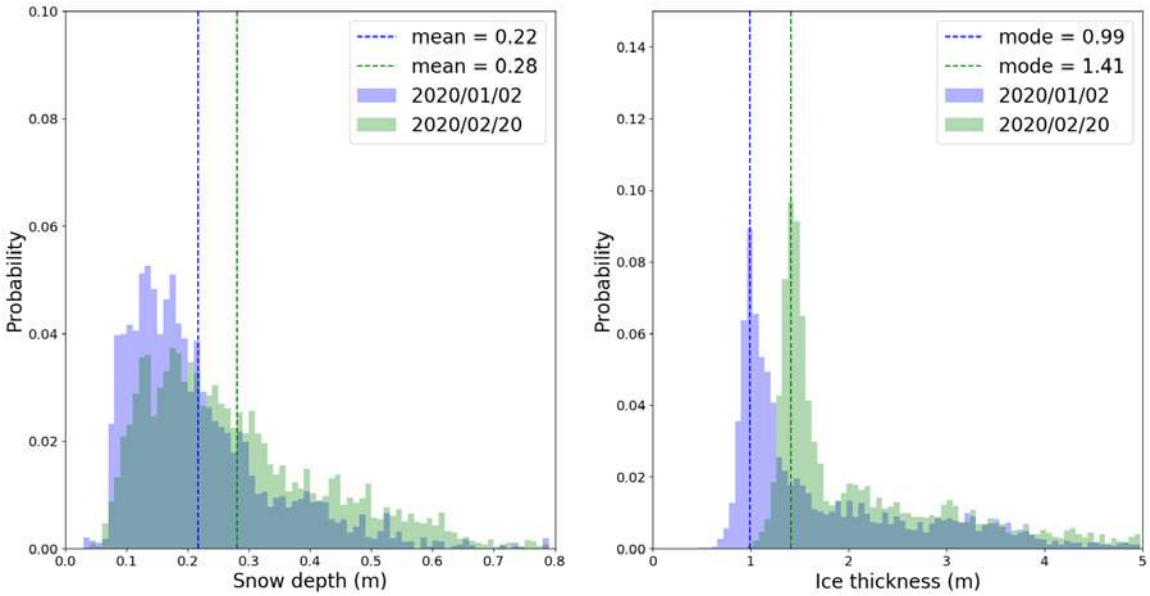

Figure S2. Snow (left) and ice thickness (right) distributions as measured by a Magna Probe (Snow Hydro) and an electromagnetic sounding device GEM-2 (Geophex) on the two main transect loops on the MOSAiC floe. Blue colors indicate a survey from 2 January 2020 coinciding with the first platelet ice observations, while green colors represent the situation on 20 February 2020. Data provided by Stefan Hendricks, AWI.

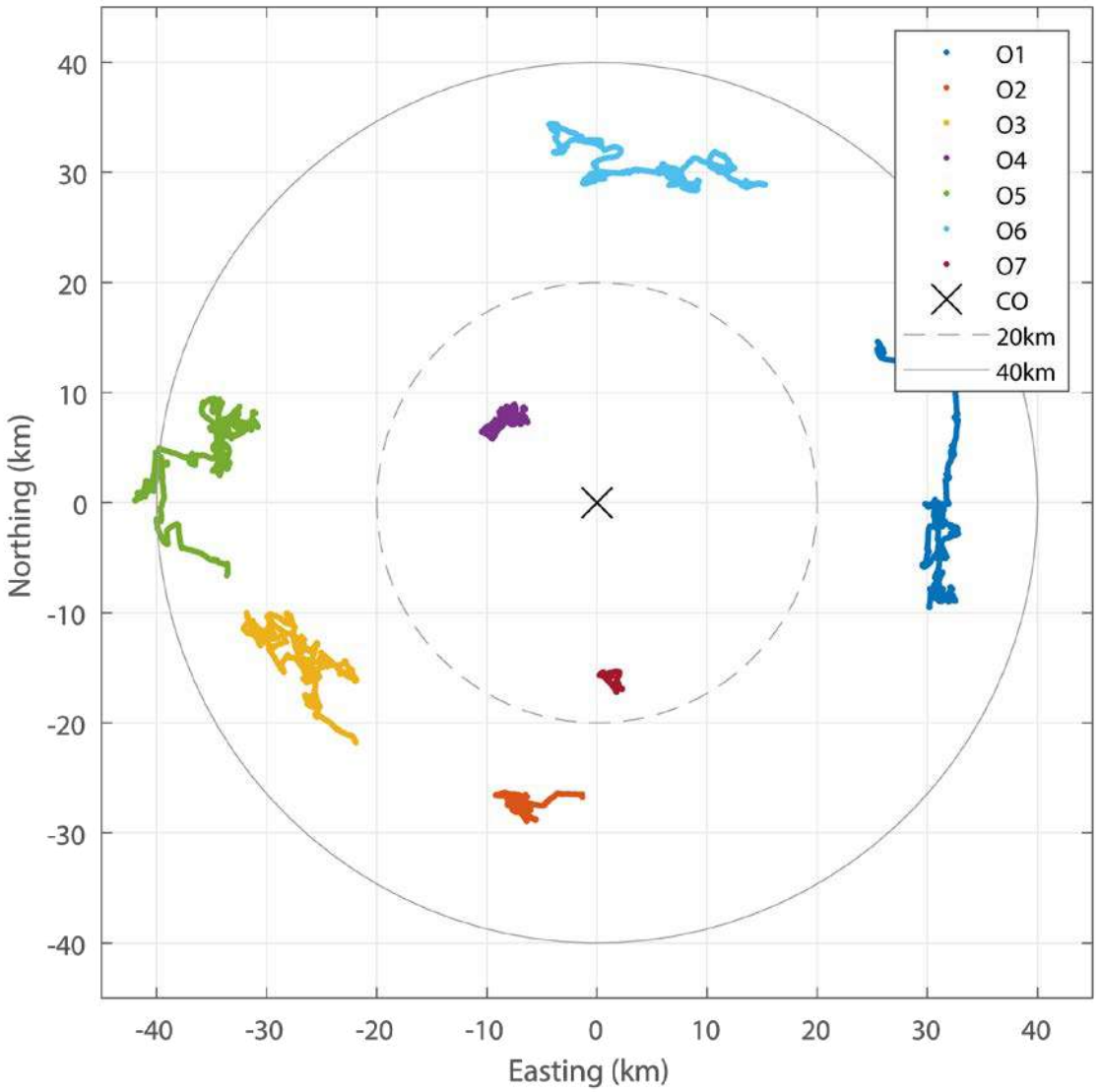

Figure S3. Relative locations of oceanographic autonomous observatories (O1-O7) in relation to the MOSAiC central observatory (CO). Plot is corrected for apparent rotation, as the MOSAiC floe drifts across a wide range of latitudes.

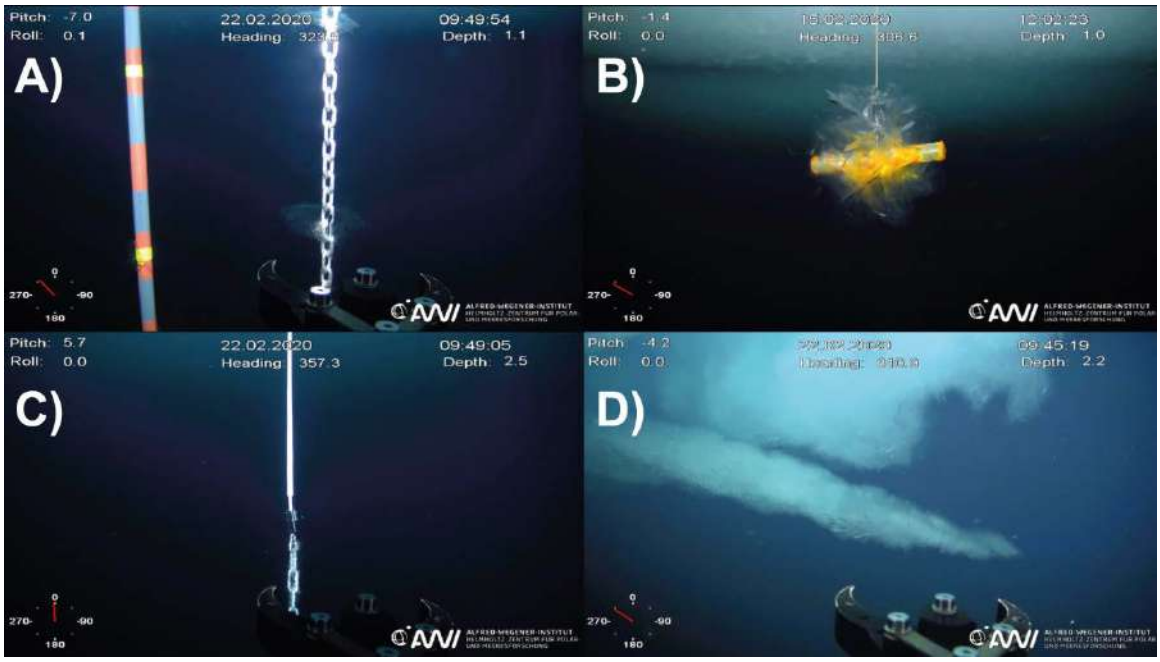

Figure S4. A) A 12 cm large single platelet crystal intergrown into a stainless steel chain. B) Platelet crystals growing around the 20 cm long steel cross-bar of a hot-wire. C) Thermistor chain covered in polymer heat-shrink. Note the absence of platelet ice on the plastic surface. D). Platelet crystals growing on an extended spike without any shelter from strong currents.

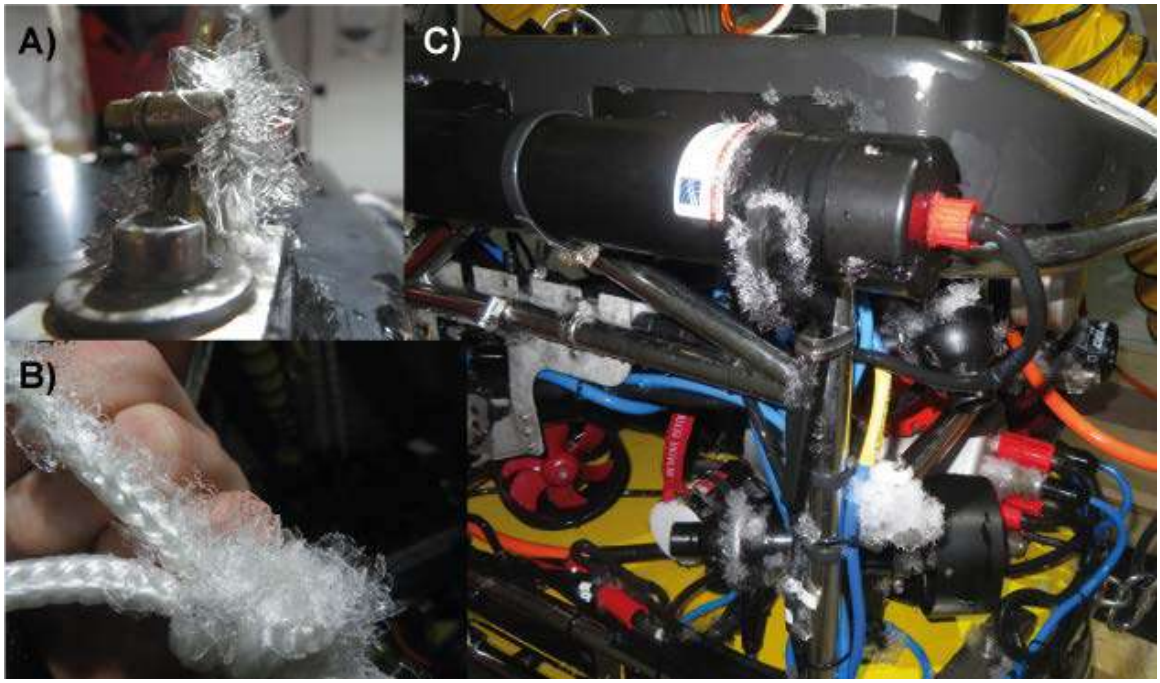

Figure S5. Platelet ice crystal growth on the ROV system: A) Close-up of small crystals on the ROV, B) Crystals growing on the attachment rope. C) Platelet growth on the edges and corners of the ROV system.

Figure S6. Vertical gradient of platelet ice growth on a chain.

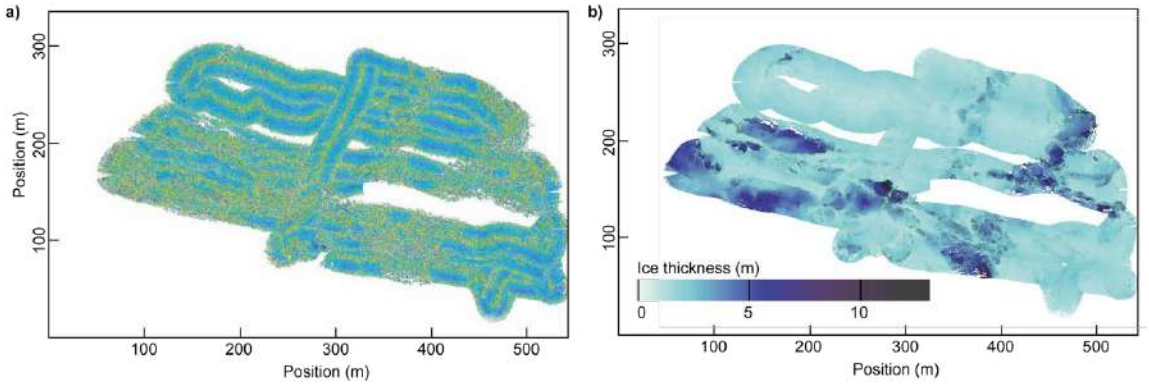

Figure S7. a) Map of raw acoustic backscatter intensity measurements on 31 December 2019. Data are not corrected for across-track incidence angle differences. Bright colors correspond to high backscatter. Regions of generally elevated backscatter are co-located with ridges as shown in the corresponding ice draft map in b). Data are available at https://doi.pangaea.de/10.1594/PANGAEA.917498.

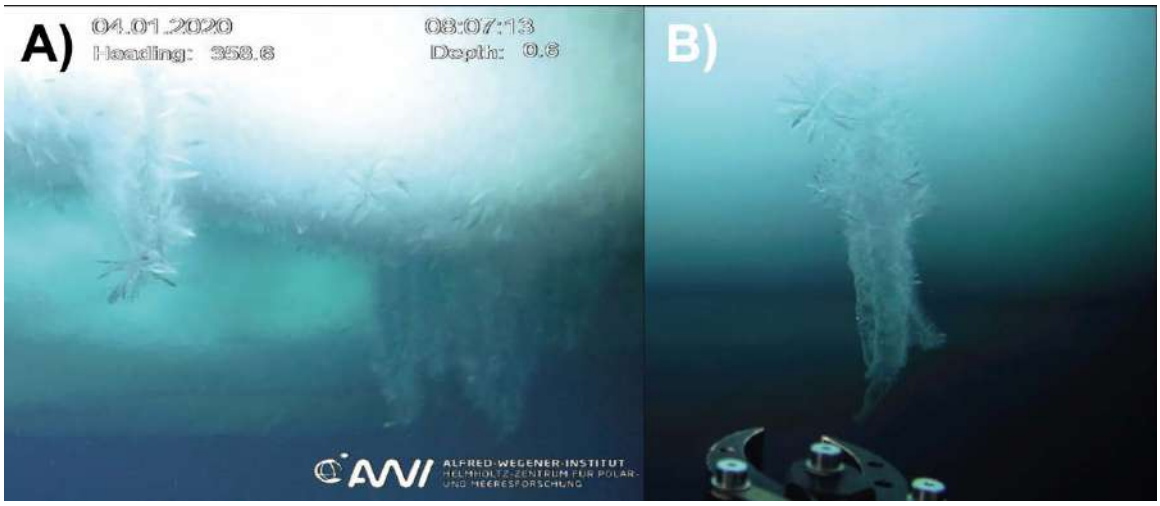

Figure S8. Brinicles under the ice observed surrounded with (A) and without (B) extensive platelet ice coverage.

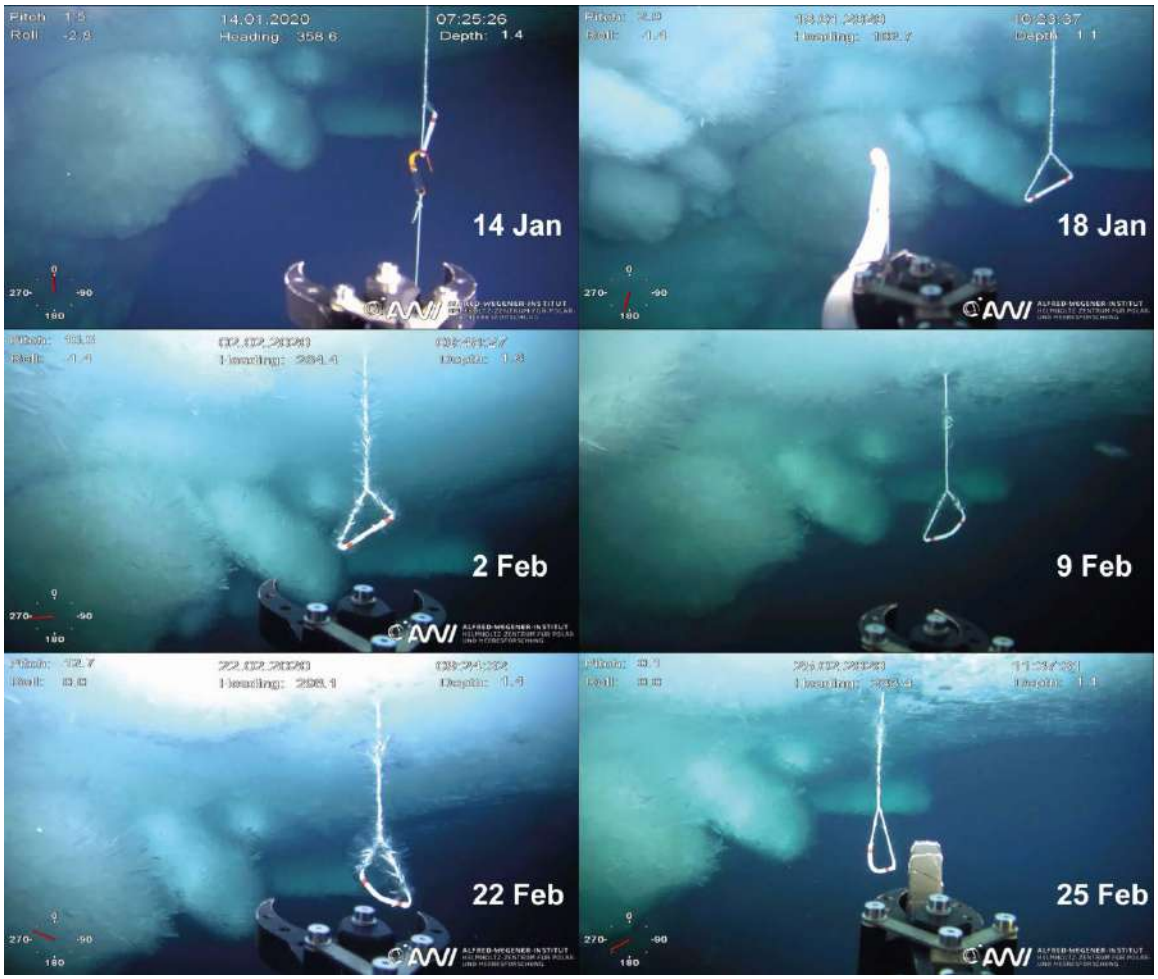

Figure S9. Time series of under-ice photographs showing the development of platelet ice on ridge blocks and a rope sling deployed next to the ridge observatory. All pictures are available at https://doi.pangaea.de/10.1594/PANGAEA.919398.

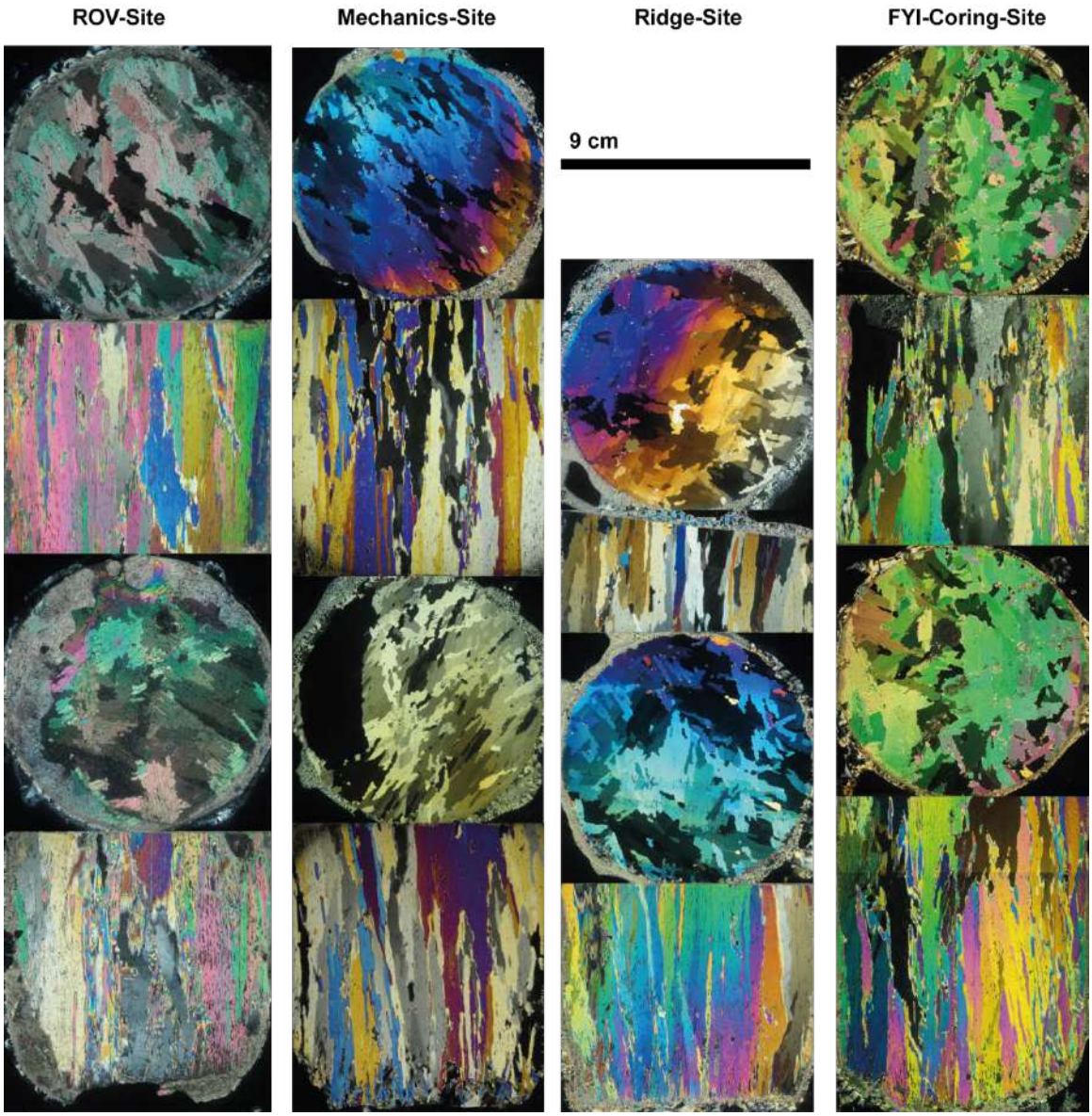

Figure S10. Thin sections of ice cores taken in the end of February photographed between crossed polarizers: horizontal (circular) and vertical thin sections of the two bottommost segments of retrieved ice cores on second year ice (thickness 1.8 m) near the ROV deployment site (left), second year ice (thickness 1.27 m) at the mechanics site (left middle), first year ice next to the ridge observatory site (thickness 1.2 m, right middle), as well as first year ice (thickness 1.23 m) at the coring site (right). Site locations are depicted in Figure 1, except the first year ice coring site which lies about 2 km away.

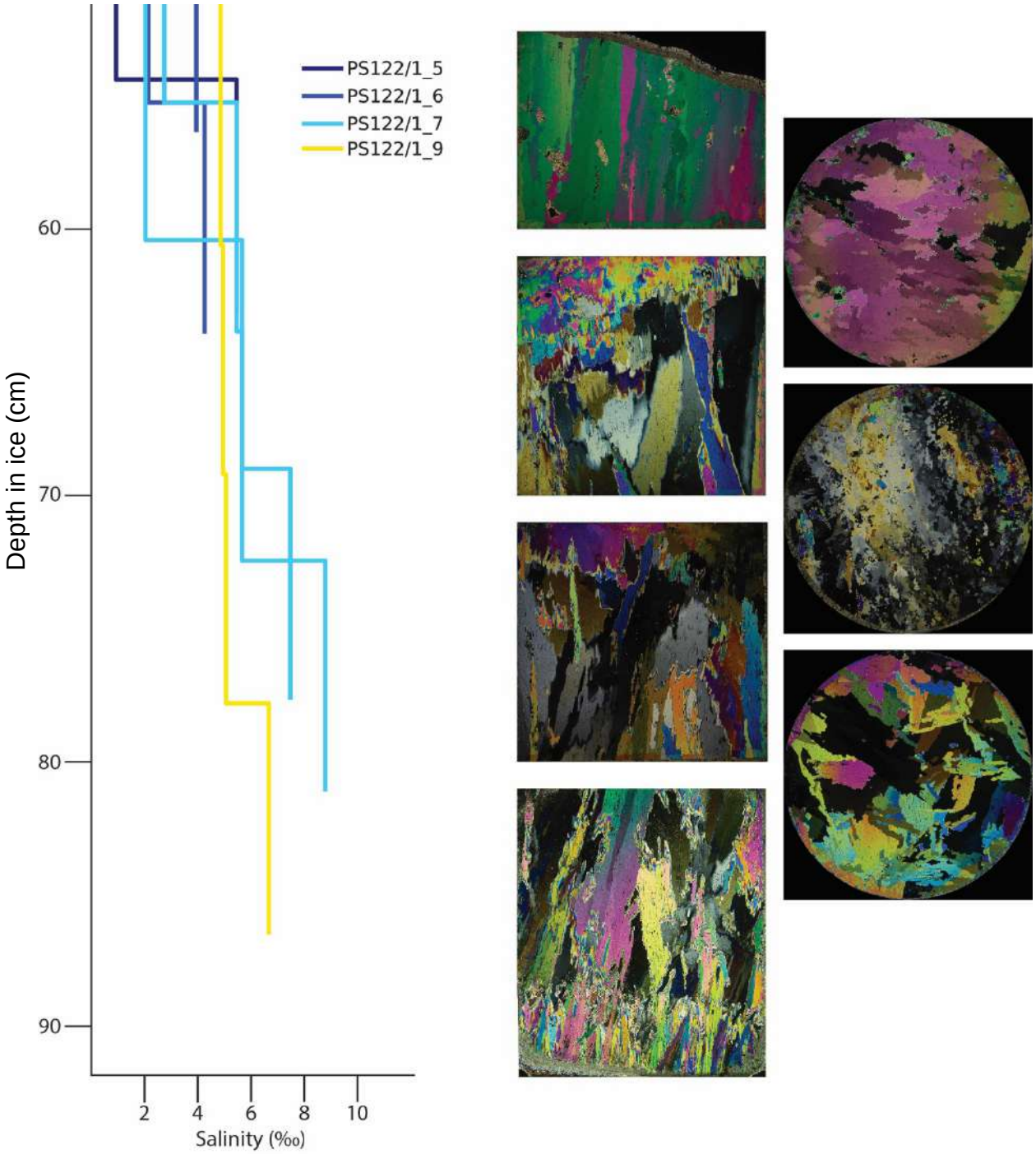

Figure S11. Bulk salinity of co-located ice cores (left) and ice stratigraphy of the lower 30 cm of an ice core collected at the second-year ice site on 25 November (PS122/1_9) before platelet ice was observed by the ROV. Vertical (rectangular) and horizontal (circular) thin sections photographed between crossed polarizers. The upper part of the core (not shown), from the surface down to about 55 cm depth, consists of remnant sea ice from the previous year. The three lower vertical sections of the ice core, starting at roughly 63 cm depth, exhibit strongly misaligned, platy crystals characteristic of platelet ice, differing substantially from columnar ice.

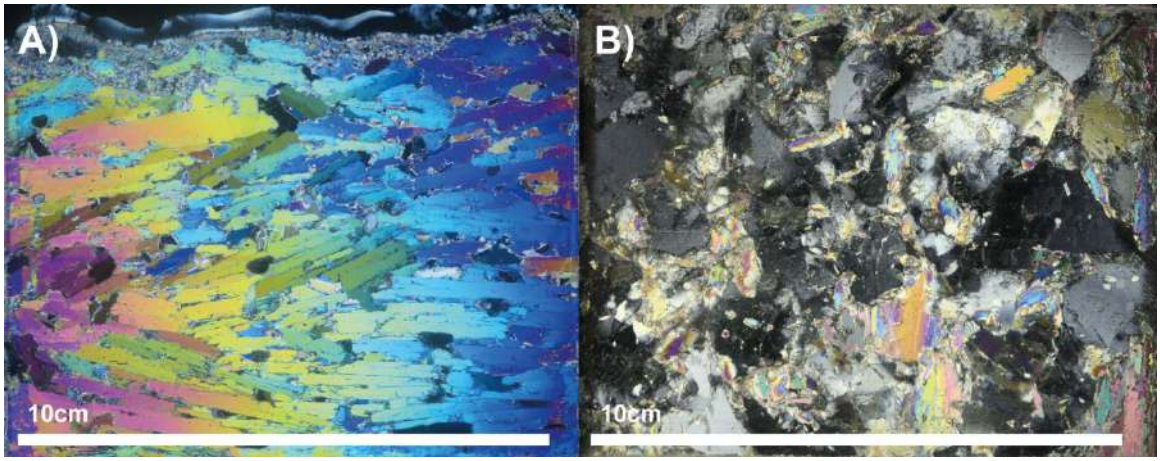

Figure S12. Thin sections of ice platelets collected with the ROVnet and refrozen with seawater in a styrofoam box photographed under crossed polarizers: A) vertical thin section showing individual platelets from the side. B) horizontal thin section showing that c-axis orientation is mostly normal to the platelet.

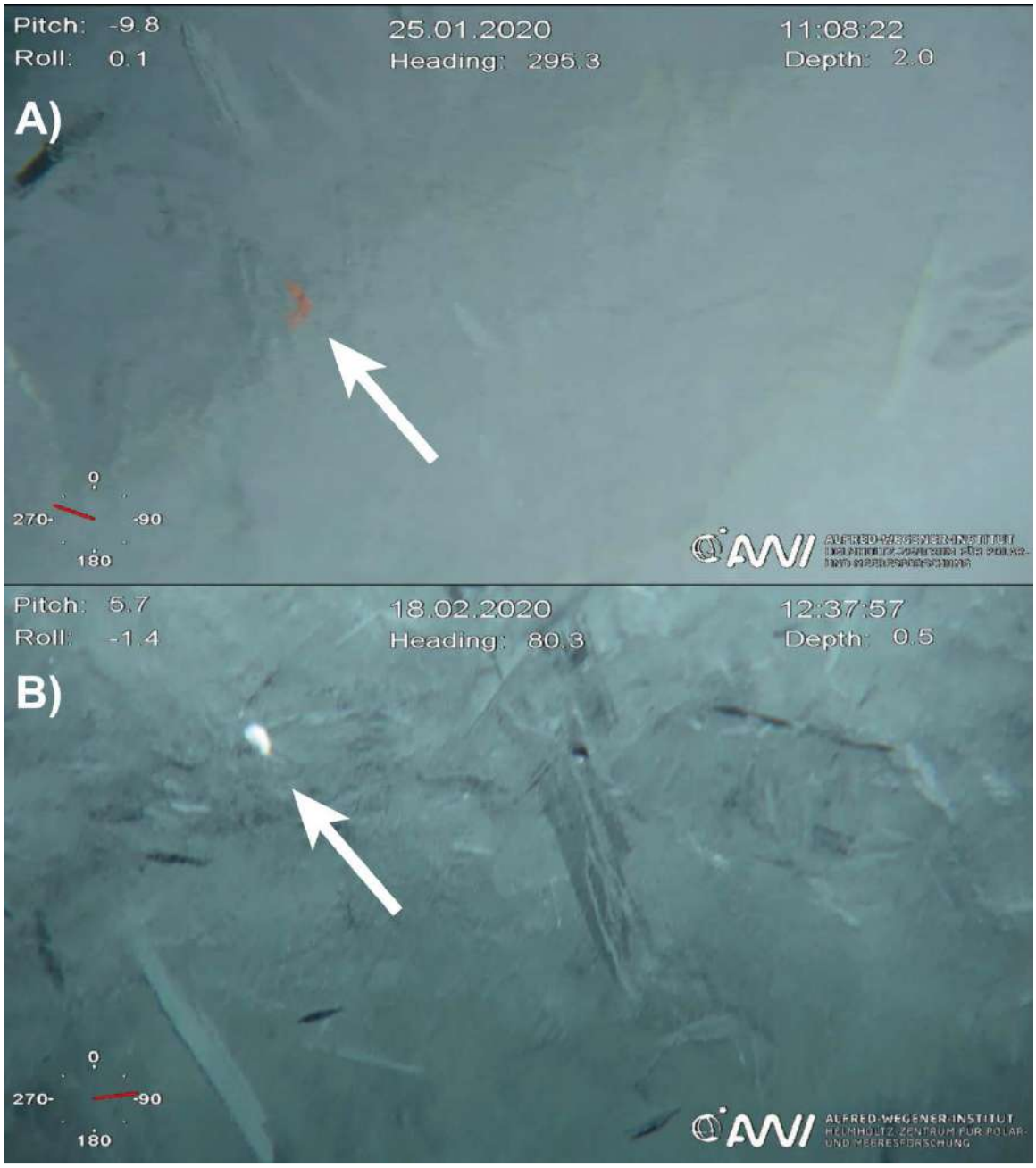

Figure S13. A&B) Under-ice macro fauna – probably amphipods – roaming in between the ice platelets.

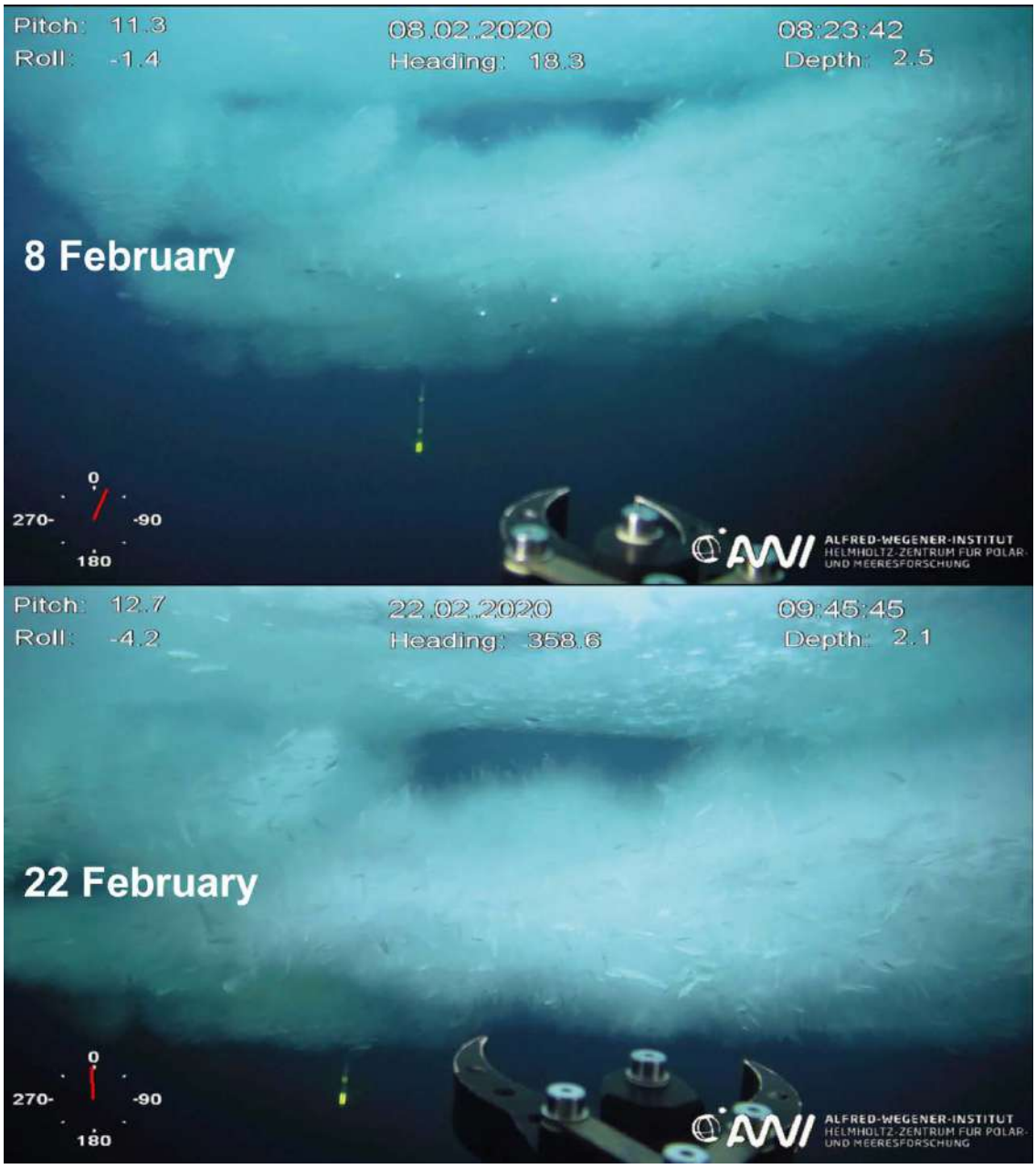

Figure S14. Time series of under-ice photographs showing the development of "upward-growing" platelet ice on top of a rafted floe.

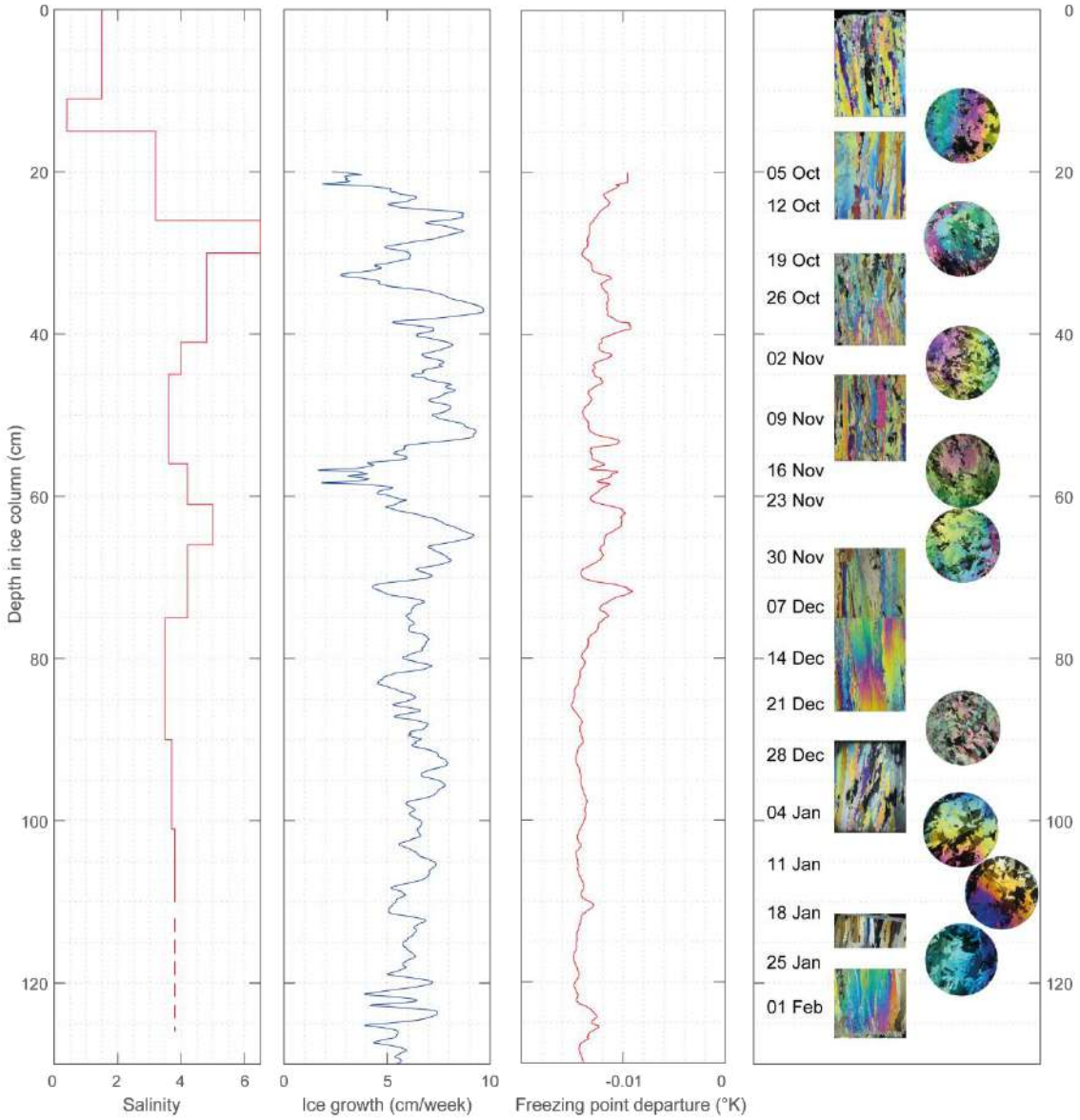

Figure S15. Analysis of the ice core retrieved on level first year ice / residual ice in the ROV survey area next to the ridge observatory. Bulk salinity (left), ice growth derived from a thermodynamic model (left middle), time-coincident freezing point departure as derived from autonomous buoy O4 (right middle). Vertical (rectangular) and horizontal (circular) thin sections along with ice formation date according to the thermodynamic model (right).

References:

Bardout, G., E. Périé, and B. Poyelle (2011), On a marché sous le pôle : Deepsea under the Pole, Chêne, [Paris].

Carnat, G., T. Papakyriakou, N. X. Geilfus, F. Brabant, B. Delille, M. Vancoppenolle, G. Gilson, J. Zhou, and J.-L. Tison (2017), Investigations on physical and textural properties of Arctic first-

year sea ice in the Amundsen Gulf, Canada, November 2007–June 2008 (IPY-CFL system study), J. Glaciol., 59(217), 819-837, doi:10.3189/2013JoG12J148.

Jeffries, M. O., K. Schwartz, K. Morris, A. D. Veazey, H. R. Krouse, and S. Gushing (1995), Evidence for platelet ice accretion in Arctic sea ice development, Journal of Geophysical Research: Oceans, 100(C6), 10905-10914, doi:10.1029/95jc00804.

Kirillov, S., I. Dmitrenko, S. Rysgaard, D. Babb, J. Ehn, J. Bendtsen, W. Boone, D. Barber, and N. Geilfus (2018), The Inferred Formation of a Subice Platelet Layer Below the Multiyear Landfast Sea Ice in the Wandel Sea (NE Greenland) Induced by Meltwater Drainage, Journal of Geophysical Research: Oceans, 123(5), 3489-3506, doi:10.1029/2017jc013672.

Lewis, E. L., and A. R. Milne (1977), Underwater sea ice formation in "Polar Oceans," paper presented at Proc. SCOR/SCAR Polar Oceans Conference, Arctic Institute North America.

McDougall, T. J., and P. M. Barker (2011), Getting started with TEOS-10 and the Gibbs Seawater (GSW) Oceanographic Toolbox, Trevor J McDougall, Battery Point, Tas.

Ragobert, T., et al. (2008), Tara : journey to the heart of the climate machine, edited.